

Article

In Situ Construction of a Co₂P/CoP Heterojunction Embedded on N-Doped Carbon as an Efficient Electrocatalyst for a Hydrogen Evolution Reaction

Ying Lei, Feng Lin, Nengyu Hong , Jian Zhang, Yulin Wang, Haijie Ben, Jianguang Li, Liyong Ding * and Liang Lv *

College of Chemical and Material Engineering, Quzhou University, Quzhou 324000, China; leiyingjy22@163.com (Y.L.); linfeng@qzc.edu.cn (F.L.); hny8066@163.com (N.H.); jianzhang6666@163.com (J.Z.); csu_lin@163.com (Y.W.); benhj@qzc.edu.cn (H.B.); 13867020905@163.com (J.L.)

* Correspondence: liyongding1988@163.com (L.D.); lianglv_buct@126.com (L.L.)

Abstract: Noble metal-free electrocatalysts have received widespread attention in a hydrogen evolution reaction (HER) due to the importance of renewable energy development. Herein, a Co₂P/CoP heterojunction embedded on an N-doped carbon (Co₂P/CoP/NC) electrocatalyst was prepared via an in situ pyrolysis method. The as-prepared electrocatalyst exhibited efficient electrocatalytic activity for HER in an acidic solution. The Co₂P/CoP/NC catalyst displayed an overpotential of 184 mV at 10 mA cm⁻² and a low Tafel slope of 82 mV dec⁻¹, which could be attributed to the tight Co₂P/CoP heterojunction and the synergetic effect of Co₂P/CoP and N-doped carbon. In addition, the electrochemical active surface area of Co₂P/CoP/NC was 75.2 m² g⁻¹, which indicated that more active regions can be applied for the HER process. This report may pave a new way for the design of efficient and low-cost N-doped-carbon-supported 3d transition metal phosphide electrocatalysts.

Keywords: Co₂P/CoP heterojunction; N-doped carbon; hydrogen evolution reaction; electrocatalyst



Citation: Lei, Y.; Lin, F.; Hong, N.; Zhang, J.; Wang, Y.; Ben, H.; Li, J.; Ding, L.; Lv, L. In Situ Construction of a Co₂P/CoP Heterojunction Embedded on N-Doped Carbon as an Efficient Electrocatalyst for a Hydrogen Evolution Reaction. *Materials* **2024**, *17*, 87. <https://doi.org/10.3390/ma17010087>

Academic Editor: Wenjie Jiang

Received: 21 November 2023

Revised: 16 December 2023

Accepted: 19 December 2023

Published: 23 December 2023



Copyright: © 2023 by the authors. Licensee MDPI, Basel, Switzerland. This article is an open access article distributed under the terms and conditions of the Creative Commons Attribution (CC BY) license (<https://creativecommons.org/licenses/by/4.0/>).

1. Introduction

Hydrogen energy is considered as a potential alternative to fossil fuels since it has advantages of high energy density, environmental sustainability, and zero carbon emission [1,2]. Electrocatalytic splitting of water is considered as one of the viable methods for continuous large-scale hydrogen production. However, with the most active Pt-based electrocatalysts, it is difficult to achieve large-scale electrolytic water splitting application due to its high cost and low earth reserves [3,4]. Thus, the development of efficient electrocatalysts with low cost, high catalytic activity, and stability is the main challenge and key research direction in the field of an electrolytic hydrogen evolution reaction.

As an earth-abundant 3d transition metal, Fe, Co, Ni, Mn, and their compound (such as sulfides, phosphides, nitrides, carbides, and oxides) electrocatalysts have been widely studied as substitutes for noble metals [5–8]. Among them, transition metal phosphides exhibited excellent electrocatalytic hydrogen evolution activity due to the high electronegativity of P atoms [7,9]. Particularly, cobalt phosphides, including Co₂P and CoP, are often used as an electrocatalyst in the HER and OER process [10,11]. Previous studies have shown that the synergistic effect of Co₂P and CoP can effectively improve the electrocatalytic activity [12,13]. Nevertheless, the synthesis methods to obtain a Co₂P/CoP nanojunction are typically complicated as well as using NaH₂PO₂ as the P source [14–17], which usually require H₂ as reduction gas or have two steps in the thermal treatment process (pyrolysis followed with the phosphating process). Therefore, one-step synthesis of a Co₂P/CoP nanojunction using simple methods is a challenging study. In addition, transition metal phosphides tend to aggregate during the synthesis process and are easily oxidized during storage [18]. In view of this, to increase the stability of transition metal

phosphides and the conductivity of the catalyst, carbon-supported nanocomposite catalysts have been developed, especially N-doped carbon materials [19]. For example, Ma et al. prepared N-doped-carbon-coated CoP nanoparticles supported on N-doped graphene through a subsequent hydrothermal treatment, pyrolysis, and a following phosphating process [18]. In another work, Chen et al. reported the preparation of CoP nanoparticles absorbed on defective reduced graphene oxide (CoP@DrGO) using $\text{NaH}_2\text{PO}_4 \cdot \text{H}_2\text{O}$ as the P source under Ar/ H_2 gas flow [11]. The synthesis process of carbon-supported cobalt phosphides typically involves multi-step reaction processes and complex control conditions. Therefore, it is imperative to find a method for synthesizing N-doped-C-supported cobalt phosphide nanomaterials. Phytic acid is an organic phosphate that can be extracted from plant seeds and has the characteristics of being green, natural, and environmentally friendly. It has been reported that it can be used as an organic phosphorus source to synthesize phosphide catalysts [7,19,20]. Polyaniline is widely used as a supporting conductive base material for catalysts due to its three-dimensional porous structure [21,22]. By adding excessive phytic acid in the synthesis process of a polyaniline precursor, the obtained polyaniline–phytic acid can be used as a conductive carbon support material and an organic phosphorus source for the synthesis of N-atom-doped-carbon-supported metal phosphide catalysts, which can reduce catalyst aggregation and oxidation, improve conductivity, and thus improve catalytic performance. In view of these, we developed a synthesis method to prepare a N-doped-carbon-material-supported $\text{Co}_2\text{P}/\text{CoP}$ nanocomposite catalyst with efficient electrocatalytic performance.

Here, a $\text{Co}_2\text{P}/\text{CoP}$ heterojunction embedded on N-doped carbon ($\text{Co}_2\text{P}/\text{CoP}/\text{NC}$) nanocomposite electrocatalysts was prepared through an in situ thermal treatment method. It should be pointed out that the synthesis process does not require additional P sources (NaH_2PO_4) or reducing gases (H_2). Moreover, the obtained $\text{Co}_2\text{P}/\text{CoP}/\text{NC}$ catalyst exhibited an exceptional synergistic effect between $\text{Co}_2\text{P}/\text{CoP}$ and N-doped C, which efficiently improved its electrocatalytic hydrogen evolution performance. This research provides a method for synthesizing high-performance 3d transition metal phosphide nanocomposite electrocatalysts.

2. Materials and Methods

2.1. Materials

Aniline ($\text{C}_6\text{H}_7\text{N}$, 99+%), Ammonium persulfate ($(\text{NH}_4)_2\text{S}_2\text{O}_8$, 98%), and Nafion (5% *w/w* in water and 1-propanol) were purchased from Alfa Aesar China (Shanghai, China). The phytic acid solution ($\text{C}_6\text{H}_{18}\text{O}_{24}\text{P}_6$, 70% in H_2O) was supplied by Aladdin (Shanghai, China). Cobalt (II) oxalate dihydrate ($\text{CoC}_2\text{O}_4 \cdot 2\text{H}_2\text{O}$, 99.7%) was provided from Macklin (Shanghai, China). Sulfuric acid (H_2SO_4 , 98%) and ethanol ($\text{C}_2\text{H}_6\text{O}$, 99.7%) were supplied by Xilong Chemical Works (Shantou, China). All chemicals were used without further purification.

2.2. Preparation of $\text{CoC}_2\text{O}_4/\text{Polyaniline-Phytic-Acid}$ ($\text{CoC}_2\text{O}_4/\text{PANI-PA}$) Precursor

The $\text{CoC}_2\text{O}_4/\text{PANI-PA}$ hybrid precursor was synthesized as follows: Initially, 0.92 mL of aniline and 1.32 mL of phytic acid (70% (*w/w*) in H_2O) were dissolved in 4 mL of deionized water with stirring to form a mixture. Then, 1.144 g of ammonium persulfate was dissolved in 2 mL of water to form a uniform solution. In total, 0.5 g of cobalt oxalate dihydrate and an ammonium persulfate aqueous solution were added into the mixture of aniline and phytic acid in turn, and the mixture was stirred for a certain time until the reaction was complete, forming a homogeneous mixture. We then allowed the mixture to undergo a complete polymerization reaction by standing at room temperature for 12 h. Finally, the mixture was washed and filtered with a small amount of deionized water and dried in an oven for about 12 h to obtain the $\text{CoC}_2\text{O}_4/\text{PANI-PA}$ hybrid precursor material.

2.3. Preparation of Electrocatalysts

The one-step synthesis of the Co₂P/CoP/NC electrocatalyst was conducted in a tube furnace. In total, 300 mg of the CoC₂O₄/PANI-PA hybrid precursor was pyrolyzed at 900 °C under a N₂ atmosphere for 2 h with a ramp rate of 5 °C min⁻¹. After the thermal reaction, the furnace was cooled down to room temperature and the Co₂P/CoP embedded on N-doped carbon nanomaterial (Co₂P/CoP/NC) was obtained. We also synthesized the samples that the CoC₂O₄/PANI-PA hybrid precursor pyrolyzed at different temperatures (800, 850, and 950 °C) and they were denoted as Co₂P₂O₇/NC, Co₂P₂O₇/Co₂P/NC, and Co₂P/NC, respectively.

2.4. Structural Characterization

X-ray diffraction (XRD) patterns were examined through an X-ray diffractometer (Rigaku D/MAX-2600, Tokyo, Japan) with Cu-K α radiation under a scanning rate of 5° min⁻¹. The Raman spectrum was collected through a Raman spectrometer (HORIBA HR Evolution, Kyoto, Japan) with a 532 nm laser as the excitation light source. The fine structures and morphologies of the catalyst were characterized by a transmission electron microscope (JEOL JEM-F200, Tokyo, Japan) and scanning electron microscope (ZEISS Gemini 300, Oberkochen, Germany) equipped with energy dispersive X-ray spectra (EDS, Smartedx, Oberkochen, Germany). X-ray photoelectron spectroscopy (XPS) was examined on a Thermo Scientific K-Alpha using a monochromatic Al K α X-ray source.

2.5. Electrochemical Characterization

All electrochemical measurements were examined on a three-electrode system using a Gamry Interface 1010E potentiostat (Gamry, Warminster, PA, USA). The electrochemical tests were conducted in 0.5 M H₂SO₄ and the catalytic electrode, Ag/AgCl electrode, and carbon rod served as a working electrode, reference electrode, and counter electrode, respectively. To prepare the catalyst ink, 4 mg of the catalysts was dispersed in the mixture of 230 μ L of H₂O, 750 μ L of ethanol, and 20 μ L of the Nafion solution with ultrasonic treatment for 30 min to form a uniform suspension. Then, 15 μ L of the catalyst suspension was loaded onto a glassy carbon electrode (5 mm in diameter) and dried naturally in room temperature to obtain the working electrode. The polarization curves were tested using linear sweep voltammetry (LSV) with a scan rate of 5 mV s⁻¹ without IR compensation in electrolytes after saturation with N₂ for 30 min. Cyclic voltammograms (CVs) were examined in the potential range of 0.1 to 0.2 V with the scan rates from 20 to 140 mV s⁻¹. All potentials in this paper were calibrated to a reversible hydrogen electrode (RHE) based on the equation $E(\text{RHE}) = E(\text{Ag}/\text{AgCl}) + 0.059 \text{ pH} + 0.197 \text{ V}$. EIS measurements were performed at -100 mV with frequency from 0.01 Hz to 100 kHz with an AC voltage of 5 mV.

3. Results and Discussion

The Co₂P/CoP/NC electrocatalyst was synthesized through one-step pyrolysis of CoC₂O₄/PANI-PA precursors. To study the growth mechanism of catalysts and synthesize high-performance catalysts, we conducted the pyrolysis process under 800, 850, 900, and 950 °C. The X-ray diffraction analysis was first performed to characterize the crystalline phase composition of the catalysts. As shown in Figure 1a, the sample obtained at 800 °C showed two obvious diffraction peaks at 29.8° and 35.3°, corresponding to the (12-2) and (130) faces of Co₂P₂O₇ (JCPDS 39-0709), respectively. When the pyrolysis temperature increased to 850 °C, two additional diffraction peaks appeared at 40.8° and 43.4°, which were ascribed to the (112) and (211) diffraction peaks of Co₂P (JCPDS 89-3030), respectively, indicating the coexistence of Co₂P₂O₇ and Co₂P. Interestingly, when the pyrolysis temperature was further increased to 900 °C, Co₂P₂O₇ was completely decomposed to form a Co₂P/CoP composite (the diffraction peaks appearing at 31.6°, 35.4°, 36.4°, 36.7°, 46.3°, 48.2°, 56.1°, and 56.8° coincide with the diffraction peaks of CoP (JCPDS 29-0497)). The XRD pattern is magnified in Figure S1 and no other diffraction peaks were found except

for Co_2P and CoP indicating there were not any byproducts in the catalyst. In addition, the diffraction peak shape of Co_2P became sharper, indicating a higher crystallinity of the sample. It is reported that the intrinsic electrocatalytic activity of CoP is higher than that of pure Co_2P , while Co_2P has better conductivity during the electrocatalytic process [23]. Thus, the presence of Co_2P can promote electron transfer performance, and the formation of a $\text{Co}_2\text{P}/\text{CoP}$ heterojunction can improve the electrocatalytic hydrogen evolution performance [17]. However, when the pyrolysis temperature was 950°C (Figure S2), the diffraction peaks of CoP disappeared, indicating that 900°C is the optimal temperature for synthesizing the $\text{Co}_2\text{P}/\text{CoP}$ mixed phase.

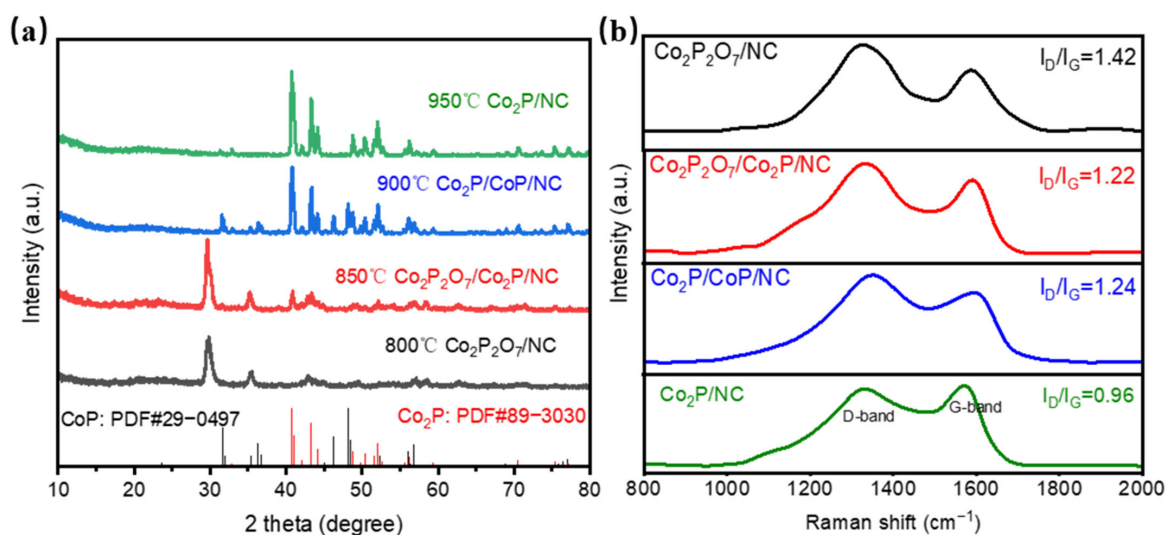


Figure 1. (a) XRD patterns of the as-prepared samples; (b) Raman spectra of the samples.

To verify the presence of carbon in the catalyst, we conducted Raman spectroscopy tests on the samples, and the result is shown in Figure 1b. Raman peaks of $\text{Co}_2\text{P}/\text{CoP}/\text{NC}$ located at 1349 cm^{-1} and 1593 cm^{-1} represented the disorder carbon (D-band) and graphitic carbon (G-band), respectively. The higher D band intensity indicated that more defects were generated [11,24]. Meanwhile, the intensity ratio (I_D/I_G) of $\text{Co}_2\text{P}_2\text{O}_7/\text{NC}$, $\text{Co}_2\text{P}_2\text{O}_7/\text{Co}_2\text{P}/\text{NC}$, $\text{Co}_2\text{P}/\text{CoP}/\text{NC}$, and $\text{Co}_2\text{P}/\text{NC}$ was 1.42, 1.22, 1.24, and 0.96, respectively. The result presented the graphitization of carbon domains formatted as the synthesis temperature increases, which can help the transfer of electrons. As a support material of transition metal phosphide, it can provide more catalytic active sites for the electrocatalytic hydrogen evolution reaction, and it is easier to adsorb hydrogen ions as well as desorb hydrogen, thereby improving the catalytic activity of the material.

The surface elemental composition of $\text{Co}_2\text{P}/\text{CoP}/\text{NC}$ was analyzed through X-ray photoelectron spectroscopy (XPS). The full XPS survey spectrum in Figure S3 revealed the existence of C, N, O, P, and Co elements in the catalyst. The high-resolution spectrum of O 1s is shown in Figure S4 and it can be deconvoluted into two peaks at 531 and 532.4 eV, which were attributed to the zero valence state and negatively charged oxygen atoms. The presence of the oxygen element is due to the inevitable partial oxidation of the catalyst in the air. The high-resolution spectrum of C 1s resolved into three peaks located at 284.6 eV, 285.5 eV, and 288.8 eV (Figure 2a), which were attributed to C-C, C-P, and C-N, respectively [25]. The N 1s high-resolution spectrum in Figure 2b could be deconvoluted into three peaks at 398.8 eV, 400.2 eV, and 401.1 eV, which were ascribed to pyridinic-N, pyrrolic-N, and graphitic-N, respectively [26]. It has been reported that the existence of graphitic-N can greatly promote the charge transfer efficiency of a catalyst, thus improving the conductivity of the catalyst. The C 1s and N 1s spectra fitting results showed that the N element was successfully doped into the carbon matrix to form the N-doped carbon framework. The high-resolution spectrum of Co 2p for $\text{Co}_2\text{P}/\text{CoP}/\text{NC}$

in Figure 2c demonstrated the Co $2p_{3/2}$ binding energies located at 779.5 eV and 781.3 eV with one satellite peak centered at 786 eV, and the Co $2p_{1/2}$ binding energies located at 794.5 eV and 797.3 eV with one satellite peak at 802.7 eV [15,23,27]. The peaks located at 779.5 eV and 794.5 eV were attributed to the Co-P bonds in the $\text{Co}_2\text{P}/\text{CoP}/\text{NC}$ catalyst, and the peaks at 781.3 eV and 797.3 eV were distributed to the Co-O bonds, which was caused by the inevitable surface oxidation of $\text{Co}_2\text{P}/\text{CoP}$. The high-resolution spectrum of P 2p in Figure 2d displayed three peaks located at 129.8 eV, 132.9 eV, and 133.9 eV that were assigned to the Co-P, P-C, and Co-O-P, respectively [28,29]. The P 2p spectrum confirmed the existence of Co-P as well as the close interaction between C and P in the $\text{Co}_2\text{P}/\text{CoP}/\text{NC}$ catalyst. The XPS spectra of $\text{Co}_2\text{P}_2\text{O}_7/\text{NC}$, $\text{Co}_2\text{P}_2\text{O}_7/\text{Co}_2\text{P}/\text{NC}$, and $\text{Co}_2\text{P}/\text{NC}$ were also characterized and are illustrated in Figures S5–S9, which can further confirm the formation of $\text{Co}_2\text{P}_2\text{O}_7/\text{NC}$, $\text{Co}_2\text{P}_2\text{O}_7/\text{Co}_2\text{P}/\text{NC}$, and $\text{Co}_2\text{P}/\text{NC}$ at different temperatures.

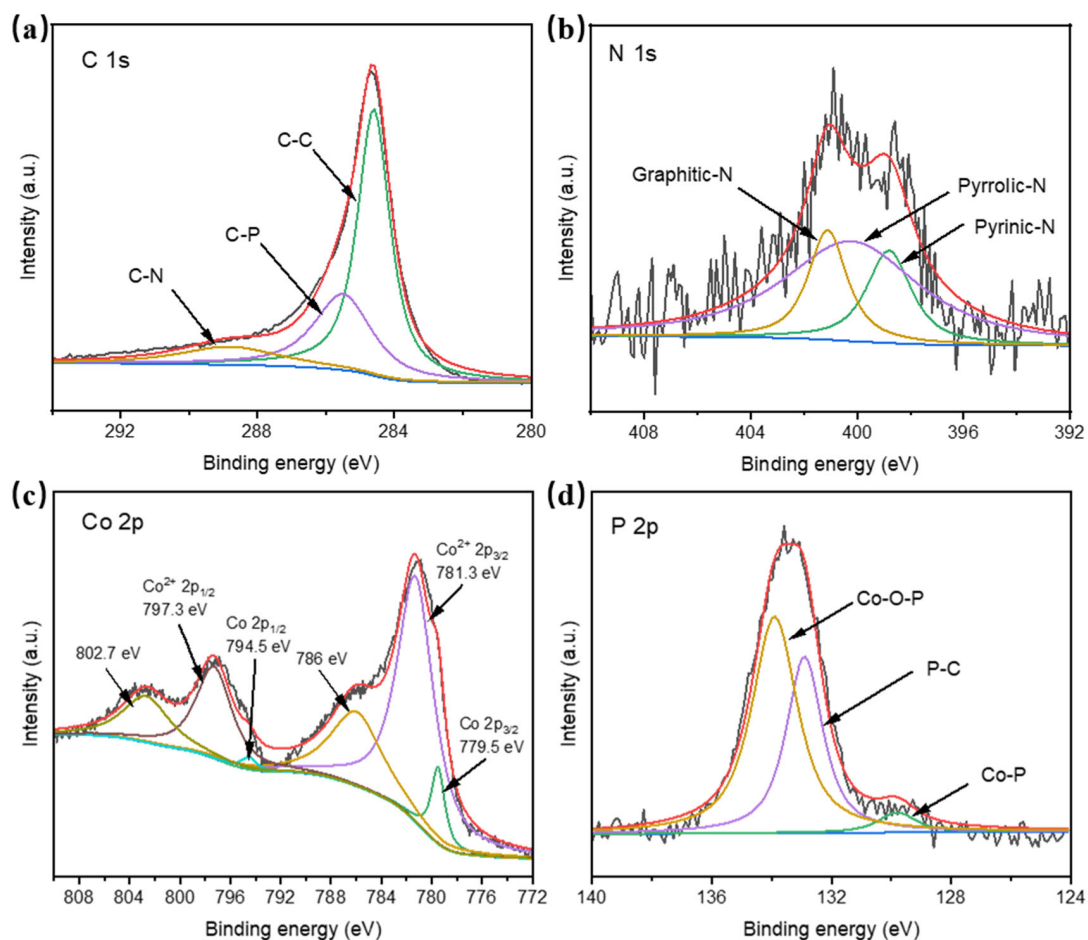


Figure 2. Deconvoluted XPS profiles of (a) C 1s, (b) N 1s, (c) Co 2p, and (d) P 2p of $\text{Co}_2\text{P}/\text{CoP}/\text{NC}$.

The morphology and nanostructure of $\text{Co}_2\text{P}/\text{CoP}/\text{NC}$ were studied through SEM and TEM. The SEM images in Figure 3a,b show a three-dimensional porous interconnected nanostructure with a diameter of about 100 nm. The TEM images in Figure 3c and Figure S10–S12 show the $\text{Co}_2\text{P}/\text{CoP}$ nanoparticles were embedded on N-doped carbon. The high-resolution TEM image in Figure 3d shows well-defined lattice fringes of 0.196 nm corresponding to the crystal plane of CoP (112). The layered structure at the edge with the lattice fringes of 0.35 nm corresponded to the (002) lattice planes of graphitic carbon [26]. The EDS spectrum of $\text{Co}_2\text{P}/\text{CoP}/\text{NC}$ is shown in Figure S13, and C, O, Co, and P were detected. Meanwhile, the atomic ratio of Co to P was calculated to be 1.73:1, indicating the coexistence of Co_2P and CoP. The EDS element mapping in Figure 3e displays the C, N, Co, and P elements in the catalyst, and the element mappings of Co and P confirmed

the formation of Co₂P/CoP embedded on N-doped carbon, which is consistent with the XPS analysis.

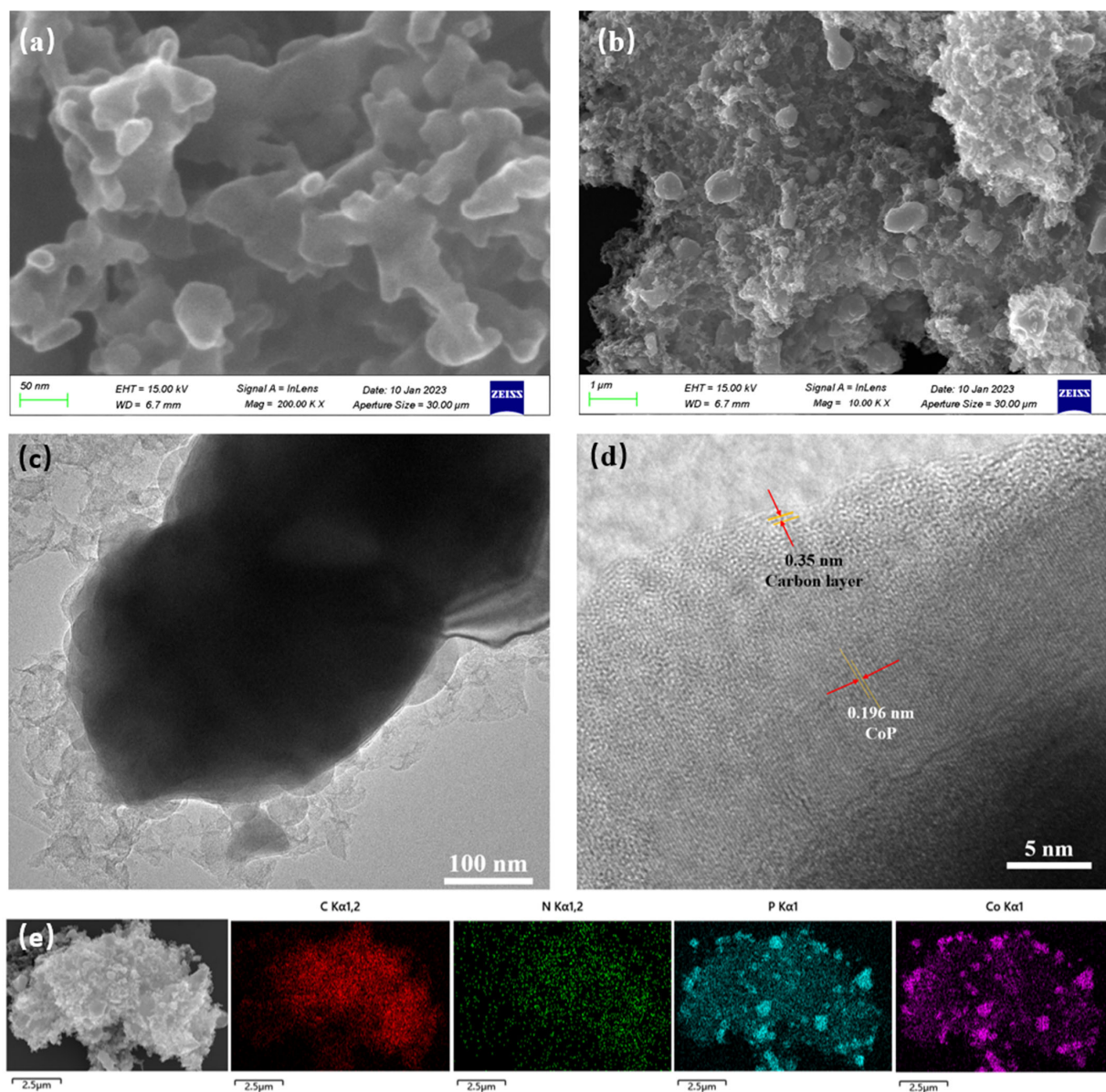


Figure 3. (a,b) SEM images of Co₂P/CoP/NC; (c,d) TEM images of Co₂P/CoP/NC at different magnifications; (e) EDS element mapping of Co₂P/CoP/NC.

To explore the electrocatalytic performance of the electrocatalysts, the HER was conducted in a three-electrode system, and commercial Pt/C (20 wt%) was selected as a comparison. Figure 4a shows the LSV curves of Pt/C, Co₂P/NC, Co₂P/CoP/NC, Co₂P₂O₇/Co₂P/NC, and Co₂P₂O₇/NC at a scan rate of 5 mV/s without iR correction. Obviously, the Pt/C catalyst demonstrated the supreme HER activity with the lowest overpotential of 41 mV at a current density of 10 mA cm⁻². Moreover, Co₂P/CoP/NC displayed an overpotential of 184 mV at 10 mA cm⁻², which was lower than that of Co₂P/NC (261 mV), Co₂P₂O₇/Co₂P/NC (241 mV), and Co₂P₂O₇/NC (395 mV). Through comparison, it was found that the electrocatalysts with Co₂P and CoP coexisting had the highest HER performance, indicating the efficient catalytic activity of Co₂P/CoP/NC. In order to further verify the optimal amount of CoC₂O₄•2H₂O added for the synthesis of catalysts, we compared the HER activity of the catalysts when 0.3 g, 0.5 g, and 1 g of

$\text{CoC}_2\text{O}_4 \bullet 2\text{H}_2\text{O}$ were added to synthesize $\text{Co}_2\text{P}/\text{CoP}/\text{NC}$ at $900\text{ }^\circ\text{C}$, respectively. As shown in Figure S14, when the addition amount of $\text{CoC}_2\text{O}_4 \bullet 2\text{H}_2\text{O}$ is 0.3 g , the overpotential at 10 mA cm^{-2} is 332 mV , while when the addition amount is 1 g , the overpotential is 250 mV . The lowest overpotential is found at the addition amount of 0.5 g , indicating that the optimal $\text{CoC}_2\text{O}_4 \bullet 2\text{H}_2\text{O}$ addition amount is 0.5 g , which means that the optimal synthesis condition for the catalyst is at a temperature of $900\text{ }^\circ\text{C}$ with a $\text{CoC}_2\text{O}_4 \bullet 2\text{H}_2\text{O}$ addition of 0.5 g , under which the catalyst has the best HER performance. To better compare the HER activities, the Tafel plots fitted from the LSV curves according to the Tafel equation ($\eta = b \log(j) + a$, where b is the Tafel slope) are shown in Figure 4b. Pt/C showed a Tafel slope of 27 mV dec^{-1} , which is similar to the values in previous literature. The Tafel slope of $\text{Co}_2\text{P}/\text{CoP}/\text{NC}$ was 82 mV dec^{-1} , indicating the HER behavior occurred on the $\text{Co}_2\text{P}/\text{CoP}/\text{NC}$ surface following a Volmer–Heyrovsky mechanism. Moreover, the Tafel slope of $\text{Co}_2\text{P}/\text{CoP}/\text{NC}$ was much lower than that of $\text{Co}_2\text{P}/\text{NC}$ (120 mV dec^{-1}), $\text{Co}_2\text{P}_2\text{O}_7/\text{Co}_2\text{P}/\text{NC}$ (121 mV dec^{-1}), and $\text{Co}_2\text{P}_2\text{O}_7/\text{NC}$ (187 mV dec^{-1}), suggesting faster reaction kinetics of HER on $\text{Co}_2\text{P}/\text{CoP}/\text{NC}$. To estimate the stability of the $\text{Co}_2\text{P}/\text{CoP}/\text{NC}$ catalyst, the long-term cyclic voltammetry (CV) measurement was conducted. As shown in Figure 4d, after 3000 CV cycles, the LSV curve of $\text{Co}_2\text{P}/\text{CoP}/\text{NC}$ showed minimal performance degradation, indicating the stability of the catalyst. Meanwhile, we also tested the chronoamperometric response curve of $\text{Co}_2\text{P}/\text{CoP}/\text{NC}$ at the potential of -0.190 V (Figure S15); the result also indicated a good stability of $\text{Co}_2\text{P}/\text{CoP}/\text{NC}$.

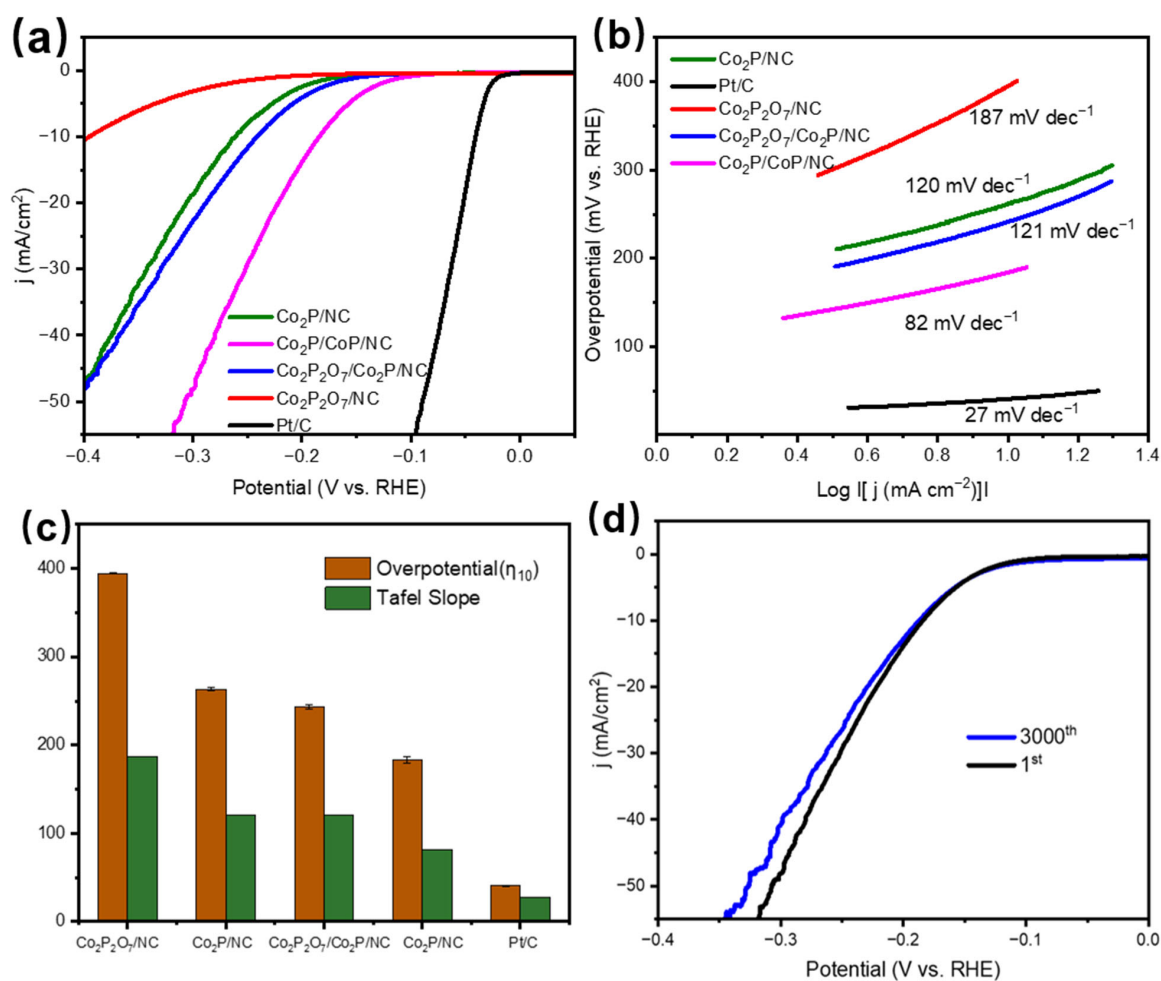


Figure 4. (a) Polarization curves and (b) Tafel plots of Pt/C, $\text{Co}_2\text{P}/\text{NC}$, $\text{Co}_2\text{P}/\text{CoP}/\text{NC}$, $\text{Co}_2\text{P}_2\text{O}_7/\text{Co}_2\text{P}/\text{NC}$, and $\text{Co}_2\text{P}_2\text{O}_7/\text{NC}$, (c) comparison of the overpotential (η_{10}) and the Tafel slope of different catalysts, (d) polarization curves of $\text{Co}_2\text{P}/\text{CoP}/\text{NC}$ before and after 3000 potential cycles.

To further investigate the mechanism of enhanced electrocatalytic hydrogen evolution performance, the electrochemical double-layer capacitance (C_{dl}) and electrochemical active surface area (ECSA) of $\text{Co}_2\text{P}/\text{CoP}/\text{NC}$ were derived by testing the CV curves at different scan rates (Figure 5a). The C_{dl} was obtained by linearly fitting Δj ($\Delta j = j_a - j_c$) at 0.15 V with the scanning rate in Figure 5b, and the C_{dl} of $\text{Co}_2\text{P}/\text{CoP}/\text{NC}$ was 13.76 mF cm^{-2} , which is comparable compared to other cobalt phosphorus compound catalysts, such as $\text{Co}_2\text{P}/\text{CoP}$ (0.434 mF cm^{-2}) [15], $\text{Co}_2\text{P}/\text{CoMoP}_x/\text{NF}$ (11.1 mF cm^{-2}) [27], and $\text{CoP}/\text{NiCoP}/\text{NC}$ (19.3 mF cm^{-2}) [6]. The ECSA of $\text{Co}_2\text{P}/\text{CoP}/\text{NC}$ was calculated in Figure S16 according to the C_{dl} , and the ECSA was $75.2 \text{ m}^2/\text{g}$ by assuming a standard value of $60 \text{ } \mu\text{F}/\text{cm}^2$. The large ECSA of $\text{Co}_2\text{P}/\text{CoP}/\text{NC}$ indicates more active regions for the electrocatalytic hydrogen evolution process.

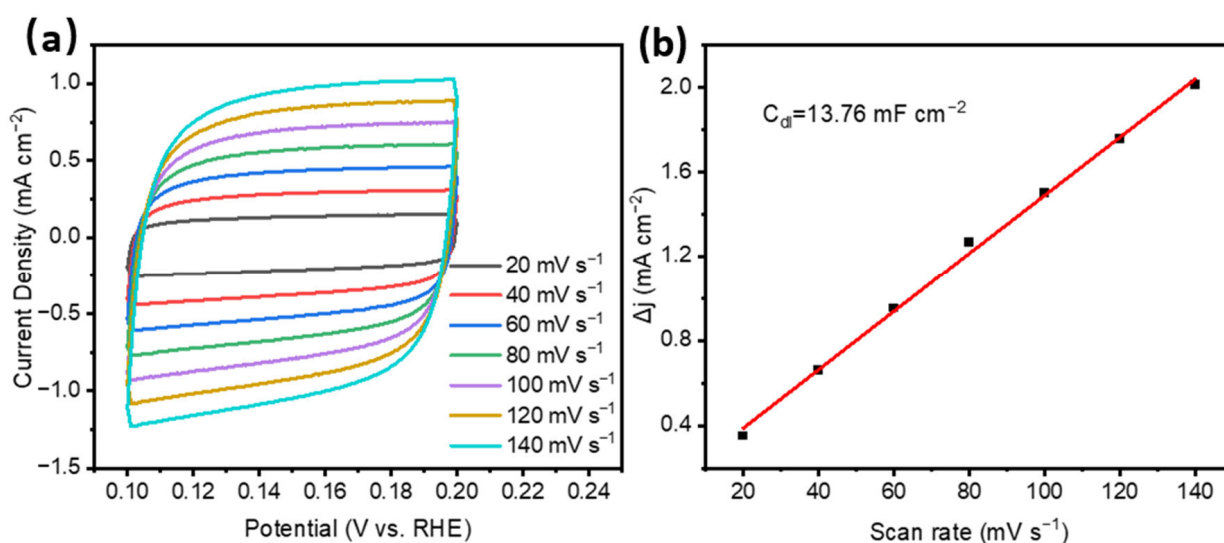


Figure 5. (a) CV curves of $\text{Co}_2\text{P}/\text{CoP}/\text{NC}$ under different scan rates, (b) extraction of electrochemical double-layer capacitance (C_{dl}) through the relationship between the current density variation (Δj) and scan rate at 0.15 V versus RHE for $\text{Co}_2\text{P}/\text{CoP}/\text{NC}$.

The EIS was performed to investigate the catalytic kinetics for HER, and Nyquist plots are shown in Figure 6. $\text{Co}_2\text{P}/\text{CoP}/\text{NC}$ presents a smaller semicircle of the Nyquist plot, which means a smaller R_{ct} and a faster electron transfer ability of the catalyst. According to the characterization results and the electrochemical studies, the electrocatalytic performance of the $\text{Co}_2\text{P}/\text{CoP}/\text{NC}$ catalyst mainly originated from the following aspects: (1) The $\text{Co}_2\text{P}/\text{CoP}$ heterojunction formed through the combination of CoP with high intrinsic electrocatalytic activity and Co_2P with good conductivity, endowing the catalyst with high electrocatalytic activity. (2) The presence of defective carbon supporting materials was beneficial to the adsorption and desorption of H^+ and H_2 , thereby improving the electrocatalytic performance. Meanwhile, the formation of N-doped C could provide a better charge transfer efficiency, resulting in high conductivity for the catalyst. (3) The high ECSA indicates that the catalyst can provide more reactive active regions and synergistic effect between Co_2P , CoP, and NC, significantly promoting the electrocatalytic hydrogen evolution performance of the catalyst.

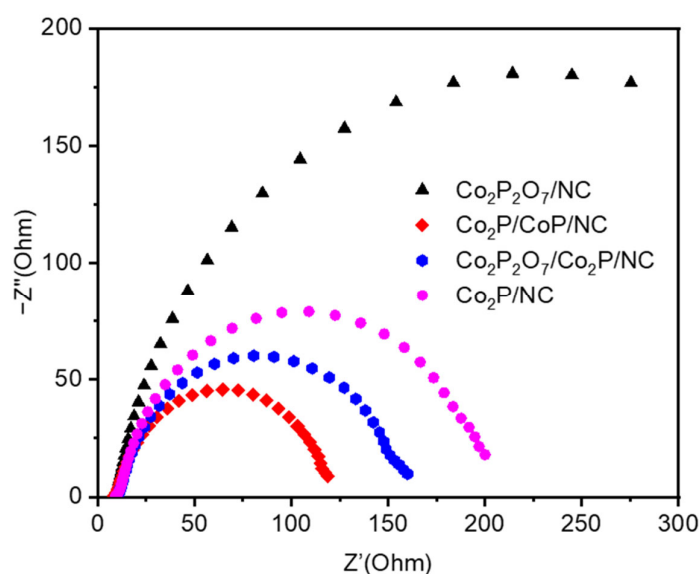


Figure 6. Nyquist plots of $\text{Co}_2\text{P}_2\text{O}_7/\text{NC}$, $\text{Co}_2\text{P}_2\text{O}_7/\text{Co}_2\text{P}/\text{NC}$, $\text{Co}_2\text{P}/\text{CoP}/\text{NC}$, and $\text{Co}_2\text{P}/\text{NC}$ at the potential of -100 mV (vs. RHE).

4. Conclusions

In this study, we successfully synthesized a $\text{Co}_2\text{P}/\text{CoP}$ heterojunction embedded on N-doped carbon nanocomposites through a pyrolysis method. The formation of $\text{Co}_2\text{P}/\text{CoP}$ heterojunctions contributes to the improvement in electrocatalytic performance, and the presence of N-doped-defective-C-supported materials helps to boost the conductivity of the catalyst and the adsorption/desorption of H^+ and H_2 , while the close contact between $\text{Co}_2\text{P}/\text{CoP}$ and N-doped C enables $\text{Co}_2\text{P}/\text{CoP}/\text{NC}$ to possess efficient electrocatalytic performance. Consequently, the $\text{Co}_2\text{P}/\text{CoP}/\text{NC}$ electrocatalyst exhibits efficient electrocatalytic hydrogen evolution ability, with an overpotential of 184 mV at 10 mA cm^{-2} , a Tafel slope of 82 mV dec^{-1} , and remarkable long-term stability. This work provides a method for synthesizing N-doped-carbon-supported iron, cobalt, and nickel phosphide nanocomposite electrocatalysts.

Supplementary Materials: The following supporting information can be downloaded at: <https://www.mdpi.com/article/10.3390/ma17010087/s1>, Figure S1. XRD pattern of $\text{Co}_2\text{P}/\text{CoP}/\text{NC}$; Figure S2. XRD pattern of $\text{Co}_2\text{P}/\text{NC}$; Figure S3. XPS survey spectrum of $\text{Co}_2\text{P}/\text{CoP}/\text{NC}$; Figure S4. Deconvoluted XPS profiles of O 1s of $\text{Co}_2\text{P}/\text{CoP}/\text{NC}$; Figure S5. C 1s XPS spectra of $\text{Co}_2\text{P}_2\text{O}_7/\text{NC}$, $\text{Co}_2\text{P}_2\text{O}_7/\text{Co}_2\text{P}/\text{NC}$, and $\text{Co}_2\text{P}/\text{NC}$; Figure S6. N 1s XPS spectra of $\text{Co}_2\text{P}_2\text{O}_7/\text{NC}$, $\text{Co}_2\text{P}_2\text{O}_7/\text{Co}_2\text{P}/\text{NC}$, and $\text{Co}_2\text{P}/\text{NC}$; Figure S7. Co 2p XPS spectra of $\text{Co}_2\text{P}_2\text{O}_7/\text{NC}$, $\text{Co}_2\text{P}_2\text{O}_7/\text{Co}_2\text{P}/\text{NC}$, and $\text{Co}_2\text{P}/\text{NC}$; Figure S8. P 2p XPS spectra of $\text{Co}_2\text{P}_2\text{O}_7/\text{NC}$, $\text{Co}_2\text{P}_2\text{O}_7/\text{Co}_2\text{P}/\text{NC}$, and $\text{Co}_2\text{P}/\text{NC}$; Figure S9. O 1s XPS spectra of $\text{Co}_2\text{P}_2\text{O}_7/\text{NC}$, $\text{Co}_2\text{P}_2\text{O}_7/\text{Co}_2\text{P}/\text{NC}$, and $\text{Co}_2\text{P}/\text{NC}$; Figure S10. TEM image of $\text{Co}_2\text{P}/\text{CoP}/\text{NC}$; Figure S11. TEM image of $\text{Co}_2\text{P}/\text{CoP}/\text{NC}$; Figure S12. TEM image of $\text{Co}_2\text{P}/\text{CoP}/\text{NC}$; Figure S13. EDS spectrum of $\text{Co}_2\text{P}/\text{CoP}/\text{NC}$; Figure S14. Polarization curves of the electrocatalysts synthesized at 900 °C with different addition of $\text{CoC}_2\text{O}_4 \cdot 2\text{H}_2\text{O}$ (0.3g, 0.5g and 1g); Figure S15. Chronoamperometric response at the potential of -0.190 V vs. the RHE; Figure S16. The calculation of ECSA for $\text{Co}_2\text{P}/\text{CoP}/\text{NC}$.

Author Contributions: Conceptualization, Y.L.; Data curation, Y.W. and H.B.; Formal analysis, N.H. and H.B.; Funding acquisition, L.D. and L.L.; Investigation, Y.L.; Methodology, N.H.; Project administration, J.L.; Resources, Y.W.; Supervision, J.L. and L.L.; Validation, F.L. and N.H.; Writing—original draft, Y.L.; Writing—review and editing, F.L., J.Z. and L.D. All authors have read and agreed to the published version of the manuscript.

Funding: This research was funded by the National Natural Science Foundation of China (No. 22106087), Zhejiang Provincial Natural Science Foundation of China (Nos. LQ22B030010 and LZY22B070001), and Research Fund for Quzhou University (No. BSYJ202102).

Institutional Review Board Statement: Not applicable.

Informed Consent Statement: Not applicable.

Data Availability Statement: Data are contained within the article and Supplementary Materials.

Conflicts of Interest: The authors declare no conflict of interest.

References

1. Zhu, B.J.; Zou, R.Q.; Xu, Q. Metal-Organic Framework Based Catalysts for Hydrogen Evolution. *Adv. Energy Mater.* **2018**, *8*, 1801193. [[CrossRef](#)]
2. Liu, Y.H.; Wang, Q.L.; Zhang, J.C.; Ding, J.; Cheng, Y.Q.; Wang, T.; Li, J.; Hu, F.X.; Yang, H.B.; Liu, B. Recent Advances in Carbon-Supported Noble-Metal Electrocatalysts for Hydrogen Evolution Reaction: Syntheses, Structures, and Properties. *Adv. Energy Mater.* **2022**, *12*, 2200928. [[CrossRef](#)]
3. Han, J.X.; Gong, C.H.; He, C.; He, P.R.; Zhang, J.; Zhang, Z.G. Sub-1 nm Pt nanoclusters on N and P co-doped carbon nanotubes for the electrocatalytic hydrogen evolution reaction. *J. Mater. Chem. A* **2022**, *10*, 16403–16408. [[CrossRef](#)]
4. Han, Y.; Duan, H.L.; Liu, W.; Zhou, C.H.; Wang, B.S.; Jiang, Q.Y.; Feng, S.H.; Yan, W.S.; Tan, T.; Zhang, R.F. Engineering the electronic structure of platinum single-atom sites via tailored porous carbon nanofibers for large-scale hydrogen production. *Appl. Catal. B-Environ.* **2023**, *335*, 122898. [[CrossRef](#)]
5. Wang, F.; Hu, L.; Liu, R.; Yang, H.; Xiong, T.; Mao, Y.; Balogun, M.S.; Ouyang, G.; Tong, Y. Hybrid implanted hybrid hollow nanocube electrocatalyst facilitates efficient hydrogen evolution activity. *J. Mater. Chem. A* **2019**, *7*, 11150–11159. [[CrossRef](#)]
6. Boppella, R.; Tan, J.; Yang, W.; Moon, J. Homologous CoP/NiCoP Heterostructure on N-Doped Carbon for Highly Efficient and pH-Universal Hydrogen Evolution Electrocatalysis. *Adv. Funct. Mater.* **2019**, *29*, 1807976. [[CrossRef](#)]
7. Pu, Z.; Amiin, I.S.; Zhang, C.; Wang, M.; Kou, Z.; Mu, S. Phytic acid-derivative transition metal phosphides encapsulated in N,P-codoped carbon: An efficient and durable hydrogen evolution electrocatalyst in a wide pH range. *Nanoscale* **2017**, *9*, 3555–3560. [[CrossRef](#)]
8. Qiang, R.; Wang, H.; Xu, K.; Yuan, Q.Y.; Yu, Y.X.; Li, L.; Wang, J.O.; Zheng, L.R.; Sherrell, P.C.; Chen, J.; et al. Available Active Sites on ϵ -Fe₃N Nanoparticles Synthesized by a Facile Route for Hydrogen Evolution Reaction. *Adv. Mater. Interfaces* **2021**, *8*, 2100070. [[CrossRef](#)]
9. Zhang, C.; Pu, Z.; Amiin, I.S.; Zhao, Y.; Zhu, J.; Tang, Y.; Mu, S. Co₂P quantum dot embedded N, P dual-doped carbon self-supported electrodes with flexible and binder-free properties for efficient hydrogen evolution reactions. *Nanoscale* **2018**, *10*, 2902–2907. [[CrossRef](#)]
10. Yuan, C.Z.; Zhong, S.L.; Jiang, Y.F.; Yang, Z.K.; Zhao, Z.W.; Zhao, S.J.; Jiang, N.; Xu, A.W. Direct growth of cobalt-rich cobalt phosphide catalysts on cobalt foil: An efficient and self-supported bifunctional electrode for overall water splitting in alkaline media. *J. Mater. Chem. A* **2017**, *5*, 10561–10566. [[CrossRef](#)]
11. Chen, Z.Q.; Wu, H.B.; Li, J.; Wang, Y.F.; Guo, W.; Cao, C.B.; Chen, Z. Defect enhanced CoP/Reduced graphene oxide electrocatalytic hydrogen production with Pt-like activity. *Appl. Catal. B Environ.* **2020**, *265*, 118576. [[CrossRef](#)]
12. Zhang, K.; Zhang, G.; Ji, Q.H.; Qu, J.H.; Liu, H.J. Arrayed Cobalt Phosphide Electrocatalyst Achieves Low Energy Consumption and Persistent H₂ Liberation from Anodic Chemical Conversion. *Nano-Micro Lett.* **2020**, *12*, 154. [[CrossRef](#)] [[PubMed](#)]
13. Gong, W.J.; Zhang, H.Y.; Yang, L.; Yang, Y.; Wang, J.S.; Liang, H. Core@shell MOFs derived Co₂P/CoP@NPGC as a highly-active bifunctional electrocatalyst for ORR/OER. *J. Ind. Eng. Chem.* **2022**, *106*, 492–502. [[CrossRef](#)]
14. Yang, Y.; Zhu, C.; Zhou, Y.; Zhang, Y.; Xie, Y.; Lv, L.; Chen, W.; He, Y.; Hu, Z. Design and synthesis Zn doped CoP/Co₂P nanowire arrays for boosting hydrogen generation reaction. *J. Solid State Chem.* **2020**, *285*, 121231. [[CrossRef](#)]
15. Zeng, Y.; Zhu, X.; Zhang, Y.; Chen, S.; Zhang, W.; Wang, L. One-step novel synthesis of Co₂P/CoP and its hydrogen evolution reaction performance in alkaline media. *Mater. Chem. Phys.* **2022**, *277*, 125419. [[CrossRef](#)]
16. Yang, J.; Guo, D.H.; Zhao, S.L.; Lin, Y.; Yang, R.; Xu, D.D.; Shi, N.E.; Zhang, X.S.; Lu, L.Z.; Lan, Y.Q.; et al. Cobalt Phosphides Nanocrystals Encapsulated by P-Doped Carbon and Married with P-Doped Graphene for Overall Water Splitting. *Small* **2019**, *15*, 1804546. [[CrossRef](#)]
17. Yi, X.L.; Song, L.Z.; Ouyang, S.X.; Wang, N.; Chen, H.Y.; Wang, J.B.; Lv, J.; Ye, J.H. Structural and Componential Engineering of Co₂P&CoP@N-C Nanoarrays for Energy-Efficient Hydrogen Production from Water Electrolysis. *ACS Appl. Mater. Interfaces* **2021**, *13*, 56064–56072. [[CrossRef](#)]
18. Ma, J.W.; Wang, M.; Lei, G.Y.; Zhang, G.L.; Zhang, F.B.; Peng, W.C.; Fan, X.B.; Li, Y. Polyaniline Derived N-Doped Carbon-Coated Cobalt Phosphide Nanoparticles Deposited on N-Doped Graphene as an Efficient Electrocatalyst for Hydrogen Evolution Reaction. *Small* **2018**, *14*, 1702895. [[CrossRef](#)]
19. Chakraborty, S.; Sahu, D.; Raj, C.R. General Approach for the Synthesis of Nitrogen-Doped Carbon Encapsulated Mo and W Phosphide Nanostructures for Electrocatalytic Hydrogen Evolution. *ACS Appl. Energy Mater.* **2020**, *3*, 2811–2820. [[CrossRef](#)]
20. Xiao, F.; Chen, Z.M.; Wu, H.; Wang, Y.; Cao, E.P.; Lu, X.D.; Wu, Y.Q.; Ren, Z.Y. Phytic acid-guided ultra-thin N,P co-doped carbon coated carbon nanotubes for efficient all-pH electrocatalytic hydrogen evolution. *Nanoscale* **2019**, *11*, 23027–23034. [[CrossRef](#)]

21. Meng, F.Y.; Yu, Y.; Sun, D.F.; Lin, S.M.; Zhang, X.D.; Xi, T.; Xu, C.M.; Ouyang, H.C.; Chu, W.H.; Shang, L.; et al. Three-Dimensional Needle Branch-like PANI/CoNiP Hybrid Electrocatalysts for Hydrogen Evolution Reaction in Acid Media. *ACS Appl. Energy Mater.* **2021**, *4*, 2471–2480. [[CrossRef](#)]
22. Huang, M.; Zhang, H.Y.; Yin, S.; Zhang, X.X.; Wang, J. PtAg Alloy Nanoparticles Embedded in Polyaniline as Electrocatalysts for Formate Oxidation and Hydrogen Evolution. *ACS Appl. Nano Mater.* **2020**, *3*, 3760–3766. [[CrossRef](#)]
23. Liu, G.; Wang, M.; Xu, Y.; Wang, X.; Li, X.; Liu, J.; Cui, X.; Jiang, L. Porous CoP/Co₂P heterostructure for efficient hydrogen evolution and application in magnesium/seawater battery. *J. Power Sources* **2021**, *486*, 229351. [[CrossRef](#)]
24. Min, S.X.; Deng, W.N.; Li, Y.N.; Wang, F.; Zhang, Z.G. Self-Supported CoP Nanoparticle-Embedded Wood-Derived Porous Carbon Membrane for Efficient H₂ Evolution in Both Acidic and Basic Solutions. *ChemCatChem* **2020**, *12*, 3929–3936. [[CrossRef](#)]
25. Boppella, R.; Park, J.; Yang, W.; Tan, J.; Moon, J. Efficient electrocatalytic proton reduction on CoP nanocrystals embedded in microporous P, N Co-doped carbon spheres with dual active sites. *Carbon* **2020**, *156*, 529–537. [[CrossRef](#)]
26. Shi, Q.; Liu, Q.; Zheng, Y.P.; Dong, Y.Q.; Wang, L.; Liu, H.T.; Yang, W.Y. Controllable Construction of Bifunctional Co_xP@N,P-Doped Carbon Electrocatalysts for Rechargeable Zinc-Air Batteries. *Energy Environ. Mater.* **2022**, *5*, 515–523. [[CrossRef](#)]
27. Chen, X.; Li, Q.; Che, Q.; Chen, Y.; Xu, X. Interface Engineering of Crystalline/Amorphous Co₂P/CoMoP_x Nanostructure as Efficient Electrocatalysts for Hydrogen Evolution Reaction. *ACS Sustain. Chem. Eng.* **2019**, *7*, 2437–2445. [[CrossRef](#)]
28. Wang, S.; Jang, H.; Wang, J.; Wu, Z.X.; Liu, X.; Cho, J. Cobalt-Tannin-Framework-Derived Amorphous Co-P/Co-N-C on N,P Co-Doped Porous Carbon with Abundant Active Moieties for Efficient Oxygen Reactions and Water Splitting. *ChemSusChem* **2019**, *12*, 830–838. [[CrossRef](#)]
29. Li, Y.; Cui, M.; Li, T.; Shen, Y.; Si, Z.; Wang, H.-G. Embedding Co₂P nanoparticles into co-doped carbon hollow polyhedron as a bifunctional electrocatalyst for efficient overall water splitting. *Int. J. Hydrogen Energy* **2020**, *45*, 16540–16549. [[CrossRef](#)]

Disclaimer/Publisher’s Note: The statements, opinions and data contained in all publications are solely those of the individual author(s) and contributor(s) and not of MDPI and/or the editor(s). MDPI and/or the editor(s) disclaim responsibility for any injury to people or property resulting from any ideas, methods, instructions or products referred to in the content.